

Efficient and Flexible Thin Film Amorphous Silicon Solar Cells on Nanotextured Polymer Substrate Using Sol-gel Based Nanoimprinting Method

Chi Zhang, Ye Song, Min Wang, Min Yin, Xufei Zhu, Li Tian, Hui Wang, Xiaoyuan Chen, Zhiyong Fan, Linfeng Lu,* and Dongdong Li*

The mechanical flexibility of substrates and controllable nanostructures are two major considerations in designing high-performance, flexible thin-film solar cells. In this work, we proposed an approach to realize highly ordered metal oxide nanopatterns on polyimide (PI) substrate based on the sol-gel chemistry and soft thermal nanoimprinting lithography. Thin-film amorphous silicon (*a*-Si:H) solar cells were subsequently constructed on the patterned PI flexible substrates. The periodic nanopatterns delivered broadband-enhanced light absorption and quantum efficiency, as well as the eventual power conversion efficiency (PCE). The nanotextures also benefit for the device yield and mechanical flexibility, which experienced little efficiency drop even after 100,000 bending cycles. In addition, flexible, transparent nanocone films, obtained by a template process, were attached onto the patterned PI solar cells, serving as top anti-reflection layers. The PCE performance with these dual-interfacial patterns rose up to 8.17%, that is, it improved by 48.5% over the planar device. Although the work was conducted on *a*-Si:H material, our proposed scheme can be extended to a variety of active materials for different optoelectronic applications.

1. Introduction

Flexible thin-film silicon solar cells are promising alternatives to bulk crystalline silicon-based photovoltaics (PVs) because of the substantially reduced processing temperature^[1] and material consumption,^[2] as well as their light weight and excellent

flexibility for portable and building-integrated applications.^[3,4] Except for the crystalline thin silicon wafer technologies,^[5,6] the thin-film silicon-based solar cells are typically produced on foreign substrates by plasma enhanced chemical vapor deposition (PECVD) methods. Although the numerous dangling bond can be effectively passivated by the intentionally incorporated hydrogen atoms, the carrier mobility (or lifetime) is still greatly lower than crystalline silicon.^[7] A reduced absorption layer thickness will increase the built-in potential and in turn benefit the electrical performance, but will limit the optical absorption capability. Therefore, utilization of state-of-the-art light management strategies to increase the optical path length within a relatively thin layer of active materials is of paramount importance for the PV community.^[8] A variety of random nanotextures^[9–11] and periodic nanostructures including nanopillars,^[12–19] nanodents,^[20–27] nanowells,^[28,29] nanopillars,^[30] nanogratings,^[31,32] and nanovoids,^[33,34] serving as back reflectors or top anti-reflection (AR) layer, have been systematically studied. A substantially improved light harvesting capability and power conversion efficiency (PCE) has been demonstrated by exciting surface plasmon resonance, photonic modes, or utilizing gradually changed effective refractive index, etc.^[13,16,21,35]

Moreover, in view of the large-scale deployment of solar cells, a cost-effective and scalable method to fabricate desirable nanostructures on flexible substrates is urgently needed. Conventional fabrication approaches for nanostructured back reflector largely rely on costly nanofabrication on rigid substrates with limited scalability.^[26,36] Sai and co-workers have demonstrated hydrogenated microcrystalline silicon (μ c-Si:H) single-junction and tandem solar cells based on the textured flexible aluminum (Al) foils.^[24,27,37] Independently, we reported a number of thin film amorphous silicon (*a*-Si:H) solar cells built on flexible Al foils with tunable nanostructures.^[17,20,21,29,38,39] Utilizing the cost-effective electrochemical anodization process, a variety of three-dimensional (3-D) back reflectors with precisely controlled pitch and height (or depth) have been realized with distinctly improved broadband absorption. Moreover, electrochemical anodization is a relatively cost-effective way

Dr. C. Zhang, Prof. Y. Song, Prof. X. Zhu
Key Laboratory of Soft Chemistry and Functional
Materials of Education Ministry
Nanjing University of Science and Technology
Nanjing 210094, China

Dr. C. Zhang, Dr. M. Wang, Dr. M. Yin, Dr. L. Tian,
Prof. H. Wang, Prof. X. Chen, Prof. L. Lu, Prof. D. Li
Shanghai Advanced Research Institute
Chinese Academy of Sciences
99 Haike Road, Zhangjiang Hi-Tech Park
Pudong, Shanghai 201210, China
E-mail: lulf@sari.ac.cn; lidd@sari.ac.cn

Prof. Z. Fan
Department of Electronic and Computer Engineering
The Hong Kong University of Science and Technology
Clear Water Bay, Kowloon, Hong Kong 999077, ChinaSAR



DOI: 10.1002/adfm.201604720

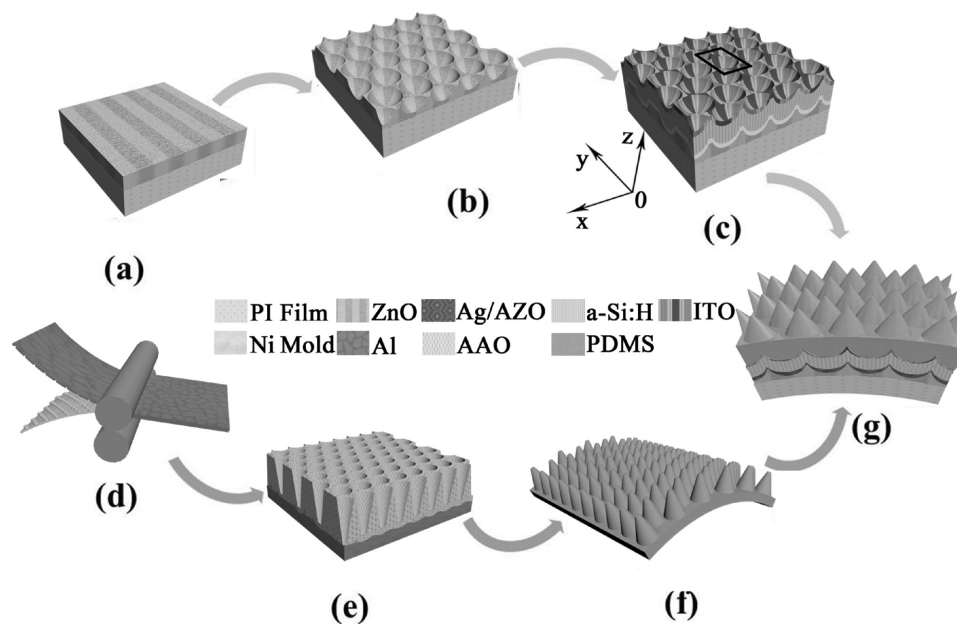


Figure 1. Schematic procedure of *a*-Si:H solar cells on patterned plastic substrates covered with nanocone AR layer. a) ZnO sol film by spin coating on PI film. b) Patterned ZnO film on PI substrate by soft thermal imprinting and post annealing. c) A *a*-Si:H solar cell constructed on the pattern ZnO/PI substrate, where the black rectangle shows the unit cell of the patterned structure. d) Formation of nanoindentation on aluminum foils by the roller-based hard imprinting. e) The porous AAO film with V-shape arrays by a multi-step anodization and wet etching process. f) The nanocone AR film peeled off from the AAO template. g) The *a*-Si:H solar cell with the patterned back reflector and top AR layer.

to fabricate nanotexture substrates and is highly compatible with the roll-to-roll production schemes. However, the devices based on aluminum foils encountered an efficiency drop of up to 7.4–8.8% under a 120° bending angle, and retained only 82–85% of the initial value after 1,000 bending cycles.^[17,20,39] Nanotextured titanium (Ti) foils, which possess a lower coefficient of thermal expansion, higher plastic deformation resistance, and temperature tolerance, have been adopted as flexible substrates. A much-improved flexibility was achieved because PCE retains 97.6% of the initial efficiency after 10,000 bending cycles (maximum bending angle is 120°).^[35] More recently, we demonstrated *a*-Si:H solar cells on plastic (polyimide, PI) films.^[40] The fabrication yield, device efficiency, and mechanical flexibility were substantially improved by introducing highly ordered nanocone structures, which benefits from the combinational effect of superior light-trapping capability and the reduction of strain/stress during thermal process and mechanical bending. However, the nanostructured films were achieved by casting liquid PI solution into the V-shape anodic aluminum oxide (AAO) molds, which is time-consuming and not compatible with large-scale production strategies.

In this work, *a*-Si:H solar cells are constructed on PI films, on which large-scale 3-D hexagonal arrays of nanoholes (NHs) are accomplished by a soft thermal nanoimprinting method using inorganically cross-linked ZnO sol-gel resists.^[41] The imprinted inorganic nanostructures possess outstanding thermal, chemical, and mechanical stability compared with conventional organic resists,^[42,43] which can be directly integrated with various thin film solar cells with high temperature tolerance. The *a*-Si:H solar cells are deposited on the 3-D nanostructures with Ag back reflector layer. In order to further boost the broadband and wide-angle light capturing capability,

an additional nanocone AR film, which offers a gradual change of effective refractive index from air to bulk material, is attached onto the top surface of the as-obtained solar cells. The optimized *a*-Si:H solar cells result in a PCE of 8.16% that is 48.5% higher than that of the flat counterpart, which is also among the highest efficiency reported for single-junction *a*-Si:H solar cells on a plastic substrate to the best of our knowledge. Moreover, the nanostructures endow the solar cells with an outstanding bendability, such that one cannot see a marginal PCE drop even after 100,000 bending cycles (bending angle = 180°).

2. Results and Discussion

Figure 1 illustrates the process flow to fabricate *a*-Si:H solar cells on patterned ZnO/PI substrates. The ZnO films with NH arrays are prepared by direct thermal nanoimprinting lithography using polydimethylsiloxane (PDMS) soft mold, as introduced in the Experimental Section. The large-scale-patterned ZnO/PI film with a size up to 8 inches was achieved as shown in **Figure 2a**. The nanosized patterns at different locations on **Figure 2a** are quite uniform, as characterized by 3D laser scanning confocal microscope (**Figure 2b**) due to the isotropic air pressure process. The larger scale optical microscope image can be found in the Supporting Information (**Figure S1**).

The surface morphology of nanopatterned ZnO films on PI substrate is further characterized by scanning electron microscopy (SEM) as shown in **Figure 2c**, in which hexagonal close-packed nanohole arrays can be clearly observed with the pitch size, hole diameter, and depth of $1\ \mu\text{m}$, $800\ \text{nm}$, and $200\ \text{nm}$, respectively. Compared to the size of master mold

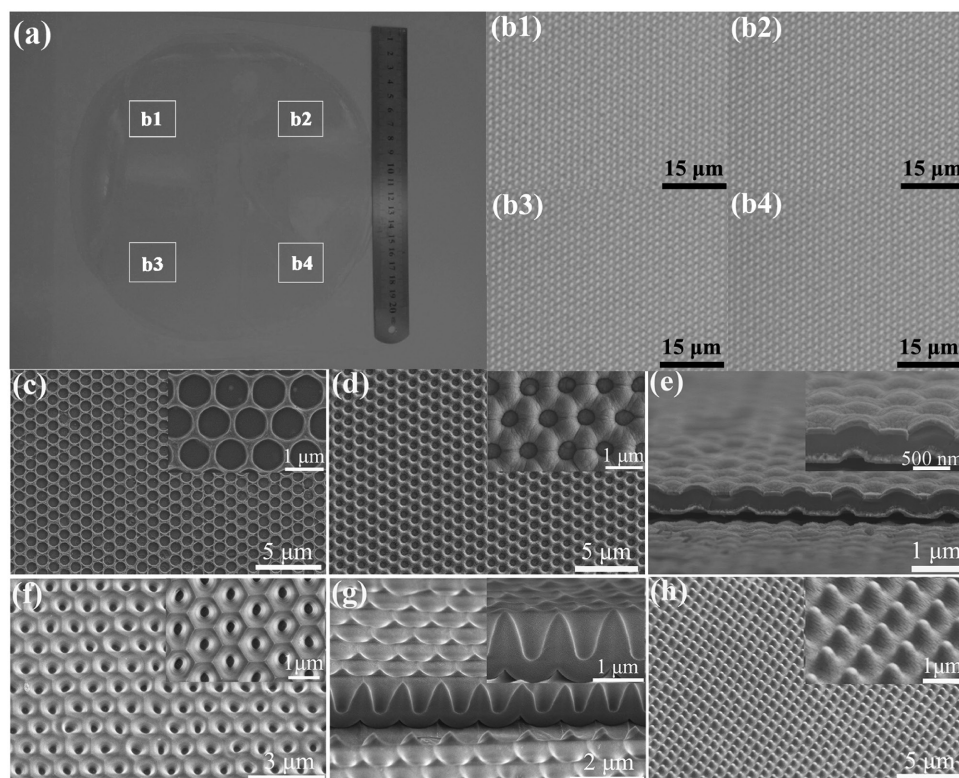


Figure 2. a) The photograph and (b1–b4) optical microscope images of the patterned ZnO/PI film. SEM images of (c) patterned ZnO layer on PI film by soft thermal imprinting, (d) top and (e) cross sectional views of *a*-Si:H solar cells fabricated on the patterned substrate, (f) top and (g) cross sectional views of AAO templates with V-shape arrays, (h) The tilted view (30°) on of flexible AR film with nanocone arrays after peeling off from AAO templates. The insets represent the corresponding enlarged images.

(pillar height = 400 nm), the depth of ZnO patterns is decreased in *z*-directions. A similar phenomenon has also been reported in previous literature due to the solvent loss.^[44,45] Thin-film *a*-Si:H solar cells are fabricated on the patterned 3D substrates and detailed fabrication processes of the solar cells can be found in our previous work.^[20,21,38,39] The photographs of solar cells on both patterned and flat substrates are shown in Supporting Information Figure S2. It has been found that the 3D substrates with high aspect ratio will generate non-uniform coverage and deteriorate device performance.^[38,39] The *a*-Si:H solar cell obtained on ZnO patterned substrate (aspect ratio = 0.25) maintains the surface morphology of hexagonal arrays with quite uniform film thickness (Figure 2d and e).

The top AR film is realized by a template process from V-shape AAO molds.^[46] Figure 2f and g show the top and cross sectional views of the highly ordered AAO template, which is fabricated by a hard imprinting process,^[17,47] and a followed multi-step anodization/wet etching process.^[38,48] Both the inter-pore distance and pore depth are about 1 μm . Figure 2h shows the AR film decorated with nanocone arrays by casting the premixed liquid PDMS into the AAO template. The nanocone structure, with both pitch size and height of around 1 μm , can not only facilitate an easy demolding process but also provide gradually changed effective refractive index. In order to investigate the optical properties of the patterned substrate, devices on both flat PI substrate and patterned PI substrates without and with PDMS nanocone film are fabricated.

The normal incident absorption spectra are measured on the devices with NH back reflector and the flat reference device as shown in Figure 3a. The optical absorption is substantially increased over the whole wavelength region after introducing the nanostructured back reflector. The enhanced optical property benefits from both broadband reduced reflection due to the nanotextured top surface (see Figure 2d and e), and efficient trapping of long wavelength light by exciting surface plasmon modes and photonic modes.^[20,21]

The optical properties are verified by electromagnetic (EM) simulation via the finite-difference-time-domain (FDTD) method shown in Figure 3b. The simulated results agree well with the experimental ones among the whole wavelength. Moreover, to understand the light propagation in the nanostructured devices, the cross-sectional electric field intensity ($|E|$) distributions within the devices are calculated as displayed in Figure 3c,d and S3, where the dashed guidelines indicate the interfaces of each functional layer. It is found that the light absorption is mainly contributed by the top layer of *a*-Si:H and ITO top contact under shorter wavelength (550 nm), as shown in Figure 3c1 and d1, and a series of finger patterns along the *z*-axis found in the flat device (Figure 3c1 and c2) originated from the interference between the incident light and the reflected light. With the presence of NH back reflector, the interference happens along both *z* and *x* directions as displayed Figure 3d1 and d2, which exhibits distinct light-trapping capability as compared with the planar one. A strong absorption is

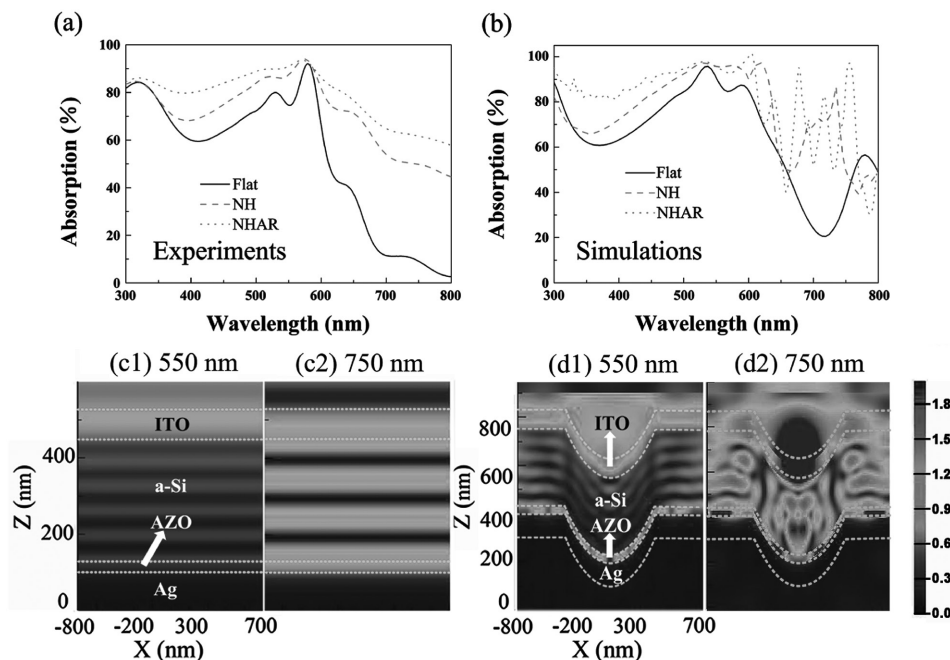


Figure 3. a) Experimental and b) simulated absorption spectra of the a-Si:H solar cells on flat and patterned PI solar cells covered without (NH device) and with (NHAR device) PDMS nanocone AR film. The cross-sectional electric field intensity ($|E|$) distributions in (c1, c2) flat and (d1, d2) NH devices at wavelengths of (c1, d1) 550 nm, (c2, d2) 750 nm, respectively.

also observed in the aluminum-doped zinc oxide (AZO) spacer layer between Ag and a-Si:H films under 750 nm illumination, which is attributed to the guided mode and lattice scattering effect.^[20] Overall, the light can be effectively confined in the patterned device, which is responsible for the improved optical absorption and is beneficial for following electron-hole pair generation and collection. Note that the optical absorption of the NH device is relatively lower than the devices obtained on nanodent back reflector accomplished by electrochemical anodization in our previous work.^[20,21,35] This could have originated from the thinner or sharper ridge along the nanodent boundaries, which determines the weakened interference effect as well as the hybrid modes consisting of cavity modes, Bloch modes, and plasmonic waveguide modes.^[35]

It was also found that an increase of the structural aspect ratio leads to a higher light absorption capability, but simultaneously with undesirable film nonuniformity, which will cause PCE degradation due to the deterioration of the internal electric field and carrier collection capability.^[17,38] As a result, the optimized 3D back reflectors typically have a moderate aspect ratio in order to depress the material defect density and carrier recombination.^[17] In order to further boost the optical performance without the deterioration of electric property, the PDMS nanocones membrane decorated with nanocone arrays is adopted on the device top surface as an AR layer. The PDMS material is chosen because of its non-toxicity, excellent optical transmittance, and good flexibility that has been adopted in light-emitting device (LED) and solar cell panel encapsulation. As shown in Figure 3a and b, the AR layer delivers a broadband light absorption enhancement thanks to the tapered nanocone shape providing a gradual change of effective refractive index from air to bulk PDMS material that depresses the front-side reflectance.

The above optical investigation shows the potency of dual-layered nanostructures for efficient photon capturing. We also noticed that the textured ZnO/PI substrate is helpful for the high quality atop layer deposition. It is known that the device fabrication process will experience heating and cooling cycles ranging from room temperature to 250 °C (see Experimental Section). The thermal cycle process will induce a stress and strain accumulation due to the large mismatches of coefficient of thermal expansion (CTE) between PI material (12–40 10⁻⁶/K)^[49,50] and other inorganic layers (Supporting Information, Table S1). As a result, macroscopic crack lines can be frequently observed from the devices on flat PI substrates (see Figure S4a). Fortunately, the patterned ZnO layer provides a larger surface area for following film deposition, which is expected to release the interface stress during the thermal cycles.^[40] Meanwhile, the nanotextured structure could also benefit from long-term stability, as the modules can reach temperatures as high as 85 °C in the real operation.^[51] Figure S4b verifies this inference with a uniform morphology on the NH device even after 5 months of fabrication.

Moreover, the PCE performances of the solar cells on nanotextured ZnO/PI substrates without (device NH) and with AR film (device NH-AR) are characterized together with the reference devices on a commercial textured FTO glass (Asahi ANS14) substrate and a flat PI substrate. Figure 4a shows current density–voltage (J – V) characteristics of the four different devices under simulated solar illumination. The corresponding short-circuit current density (J_{sc}), open circuit voltage (V_{oc}), fill factor (FF) and PCE extracted from these J – V curves are summarized in Table 1. It can be seen that the V_{oc} of the patterned PI device is slightly decreased compared to the flat counterpart. Our previous study indicated that the weaker internal electric

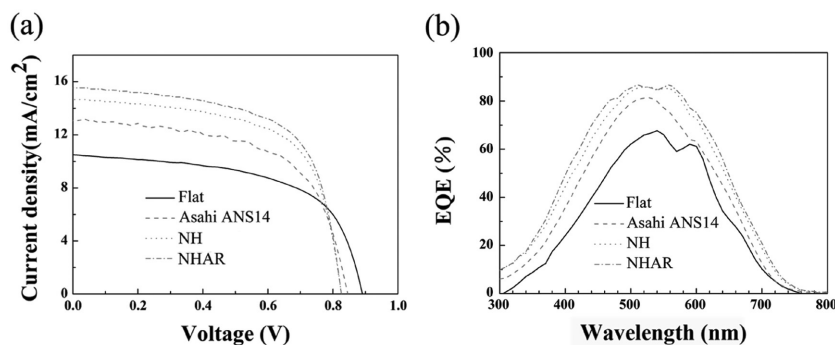


Figure 4. a) J - V curves and b) EQE measurements of a -Si:H devices based on the flat PI film, Asahi ANS14 FTO glass and PI film with ZnO-gel patterns without and with PDMS nanocone.

fields were preferred to be localized in the top corners of a unit cell. A local current reversal was observed when approaching the open circuit voltage, which is responsible for the reduction of V_{oc} on nanopatterned devices.^[52]

We also find an improved FF , which may be originated from the reduction of the series resistance (R_s) of the devices from 75.26 Ohm (flat) to 47.13 Ohm (NH).^[21,22,53] The J_{sc} increases from 10.45 mA/cm² to 13.15 and 14.69 mA/cm² using textured FTO glass and nanopatterned ZnO/PI instead of the flat PI substrate. The increased J_{sc} of the NH device can be confirmed with external quantum efficiency (EQE) measurements as shown in Figure 4b, which presents a broadband spectra response enhancement with respect to the planar reference device. As a result, the overall performance of NH device improved from 5.50% to 7.71%. After attaching the AR film (device NHAR), the J_{sc} and PCE further rose to 15.57 mA/cm² and 8.17%, which is improved by 49.0% and 48.5% over the planar device, respectively. The EQE results in Figure 4b suggest that the presence of the nanocone AR layer gives rise to a broadband spectra response enhancement that is consistent with optical absorption profiles, as shown in Figure 3a and b.

It is known that the angle of solar irradiation changes over time in a day for practical operation (Figure 5a). Therefore, the angular-dependent PCE is of special interest to the PV community. Figure 5b shows the PCEs of NH and NHAR and flat reference devices for the light incident angles changing from 0° (normal incident) to 60° with a 10° interval, where the PCE values are calculated using the device active area, regardless of the change of projection area under different incident angles. It is clearly seen that the NH and NHAR devices possess higher PCEs over all incident angles with an enhancement of ≈40% and ≈50% compared to the flat counterpart.

Table 1. Summary of device performances of four different a -Si:H solar cells.

Device	V_{oc} (V)	J_{sc} (mA/cm ²)	FF (%)	PCE (%)
Flat	0.89	10.45	0.59	5.50
Asahi ANS14	0.85	13.15	0.60	6.71
NH	0.82	14.69	0.64	7.71
NHAR	0.82	15.57	0.64	8.17

The PI material, which possesses better flexibility than metal foils^[20,35,39] and a higher temperature tolerance than polyethylene terephthalate (PET) and polyethylene naphthalate (PEN),^[54,55] is expected to be a promising choice for flexible electronics. Previously, we have demonstrated flexible solar cells based on nanotextured aluminum,^[39] titanium,^[35] and PI^[40] foils, which encountered 18% (1,000 cycles @120° bending angle), 2.4% (10,000 cycles @120° bending angle) and 4% (10,000 cycles @180° bending angle) drop of the initial efficiencies. Device performance degradation could result from the generated strain and stress in the thin films during bending, which increase the possibility of

crack nucleation and delamination at the interface of the layers. To evaluate the robustness of the PI-film-based device in this work, the PCEs of NH under a bending angle from 0° to 180° are characterized with a homemade setup.^[20] The normalized efficiencies are calculated using the device projection area. It is found that the device only experiences about 17% efficiency drop even under 180° bending angle, as shown in Figure 5c. More intriguingly, even after 100,000 bending cycles, one can hardly see a marginal drop.

It is known that the a -Si:H possesses excellent mechanical properties and has been widely employed in flexible devices.^[56,57] However, the metal oxides, including AZO and indium-doped tin oxide (ITO) are ceramic materials, which are brittle and may decrease the device flexibility. Letierrier et al.^[58] found that a thinner ITO yields a decreased internal stress and an increased crack onset strain. For instance, the crack onset strain of ITO films increased from 1.52% to 2.19% as the thickness decreased from 100 to 50 nm. In our work, the thicknesses of AZO and ITO are 30 and 80 nm, respectively, which may depress the intrinsic brittleness. Moreover, the outstanding flexibility could dominantly benefit from the preformed ZnO NH arrays on PI substrate, which provides a higher surface area in the interfacial regions between each layer and in turn induces lower stress with more uniform distribution across all functional layers.^[40]

3. Conclusion

In this work, we demonstrated highly ordered metal oxide patterns on 8-inch, flexible PI foils by a cost-effective sol-gel soft imprint process, which efficiently suppressed the internal stress during the a -Si:H solar cell fabrication and in turn is beneficial for the subsequent high-temperature deposition. The remarkable and broadband enhancements in optical absorption and quantum efficiency were realized on NH device with nanohole array back reflector. In conjunction with the nanocone AR film, a PCE value of up to 8.17% was achieved, thanks to the gradient in effective refractive index of AR film and the hybrid optical modes excited by nanotextured back reflector. Moreover, the flexibility has been also considered as a function of bending angle and bending cycle. The nanopatterned ZnO/PI substrate delivered an excellent device performance without

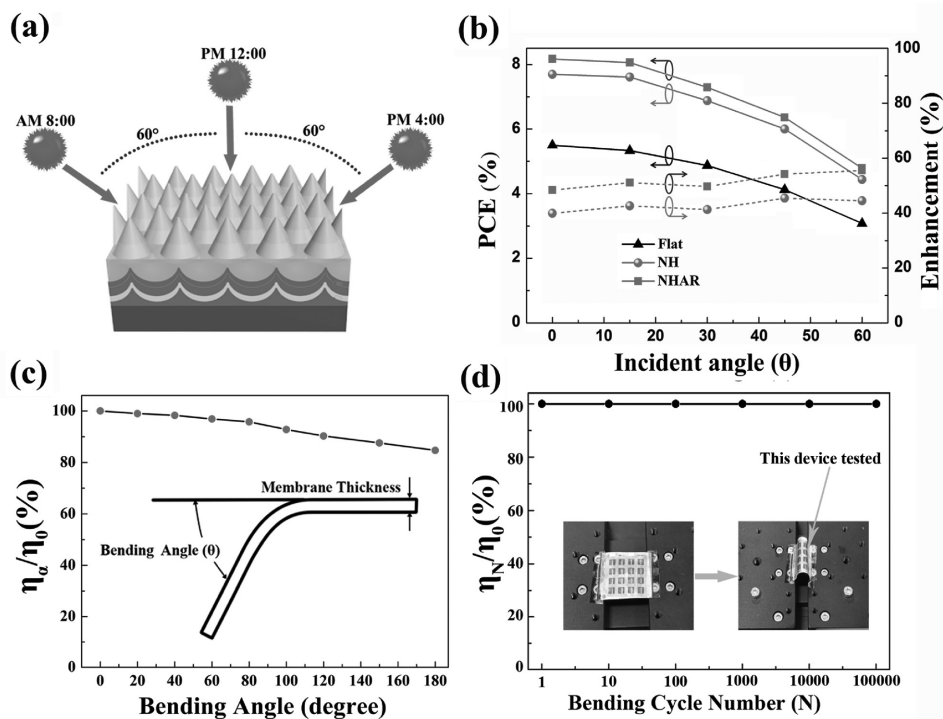


Figure 5. a) A schematic of defining incident angle. b) PCEs of NH, NHAR, and flat devices as a function of incident angles. c) Normalized efficiencies of NH devices under bending angles from 0 to 180°. d) Relative efficiency as a function of bending cycles. The insets in (c) and (d) represent an illustration of defining bending angle and a bended device mounted on the measurement setup, respectively.

marginal retention even after 100,000 bending cycles, owing to the suppressed stress across functional layers. Although the work was conducted on *a*-Si:H material, our proposed scheme can be extended to a variety of active materials for optoelectronics application. Additionally, by employing the UV-curable inorganic oxide-organic composites and roll-to-roll process, the production of photonic structures would be more efficient.

4. Experimental Section

Preparation of ZnO sol: 1 M ZnO sol was prepared by dissolving 0.1 mol of zinc acetate 2-hydrate ($Zn(CH_3COO)_2 \cdot 2H_2O$) as a precursor in 0.1 L of *N,N*-dimethylformamide (DMF) solvent medium and dropping diethanolamine (DEA) into the solution as a sol stabilizer while maintaining the molar ratio of DEA/Zn^{2+} at 1:1, then gently stirring until completely melted.^[44]

Preparation of nanopatterned ZnO/PI film by soft thermal nanoimprinting lithography: Surface-patterned ZnO thin films were realized by direct imprinting on polymeric ZnO precursor sol and subsequent annealing process.^[41] In brief, the polydimethylsiloxane (PDMS) soft molds with hexagonal closed-packed nanopillar arrays (pitch size = 1 μm, pillar diameter = 800 nm, pillar height = 400 nm) were firstly produced from Si master stamp. An anti-sticking coating process using a fluorinated silane precursor was adopted on the Si master stamp by a molecular vapor deposition process (Molecular-100S, Swind Ltd.) under 100 °C. The PDMS (Sylgard 184) stamps were subsequently prepared by casting a 10:1 weight ratio mixture of basic agent and firming agent on the Si master mold and substantially curing at 60 °C for 3 h.

The ZnO sol was spin coated on pre-cleaned PI substrate (UBE Industries, Ltd., 25 μm) at 3000 rpm for 50 s (Figure 1a). The patterned PDMS was then attached onto the obtained sol film and subjected

into a nanoimprinting chamber (NC-AX1401, Swind Ltd.). A thermal nanoimprinting process was carried out under 0.6 MPa and 250 °C for 2 h until the sols was transferred to the stable nanopatterned gels. PDMS material was chosen due to its capability to absorb the solvent without deformation.^[59] After the imprinting process, the ZnO-gel patterns on PI substrates were further cured in air at 250 °C for 2 h to remove the solvent completely.

Fabrication of *a*-Si:H Solar Cells: Thin-film *a*-Si:H solar cells were fabricated on the patterned ZnO/PI substrates. Specifically, a 100 nm Ag layer was deposited as a back reflector on the as obtained substrates by DC magnetron sputtering. Then, a AZO spacer layer, with a thickness of 30 nm, was prepared on the Ag-coated substrate by radio frequency (RF) magnetron sputtering of a 2 wt% Al_2O_3 doped ZnO ceramic target (purity 99.99%) under 250 °C. Subsequently, a stack of *n-i-p* amorphous silicon layers was fabricated in a PECVD multi-chamber system under 250 °C. The *n*- and *p*-type layers are 30 nm and 10 nm thick, respectively, while the thickness of the intrinsic *a*-Si:H layer is 280 nm. An ITO top contact (80 nm) was then deposited by RF sputtering under 250 °C. Finally, a Ag grid was thermally evaporated as the top electrode over ITO using a contact mask.^[21,38] For comparison, the solar cells were also fabricated on a commercial textured FTO glass (Asahi ANS14) substrate and a flat PI substrate under the same process.

Fabrication of top AR films: The top AR films started with an imprinted Al foil and following electrochemical anodization to form anodic aluminum oxide (AAO) with V-shape nanopore arrays. Flexible nickel nanoimprint master with hexagonally ordered nanopillars is fabricated by nanoimprint lithography and electroplating. Sequentially, imprinted Al foil is achieved by roll-to-roll nanoimprint. Detailed information on the fabrication of flexible nickel stamp, imprinting process, and anodization parameters can be found in our previous work.^[17] After obtaining the AAO template, a fluorinated silane precursor is evaporated into the template serving as an anti-sticking layer by the molecular vapor deposition (MVD) method (Molecular-100S, SWIND Ltd.). Subsequently the premixed polydimethylsiloxane (PDMS) were poured onto the template, followed by a degas and curing process at 60°C for 3 hours.

The cured PDMS membrane with a thickness of ≈ 1 mm decorated with nanocone arrays was peeled off from the template and can be readily transferred onto the photovoltaic device as an AR window layer.

Simulations: The electromagnetic simulations were accomplished by employing the FDTD method (Lumerical FDTD solutions). The unit cell of the patterned structure was set as the simulation region using anti-symmetrical boundaries in the x-axis, symmetrical boundaries in the y-axis and perfectly matched layer (PML) boundary conditions in the z-axis.^[21] A plane-wave light source irradiated normally to the device was set to be transverse magnetic (TM) polarized considering the hexagonal arranged structure is polarization insensitive, while one monitor was placed between the source plane and device surface in order to detect the device absorption. Complex refractive indices of Ag and ZnO are adopted from Palik's handbook of Optical Constants^[60] while those of AZO, ITO and *n-i-p a-Si:H* are measured data as shown in Supporting Information Figure S5.

Characterization: SEM images of the samples were characterized by scanning electron microscope (SEM, Hitachi S4800). The optical reflection measurements were carried out with an integrating sphere. All the *J-V* curves of thin-film *a-Si:H* solar cells were carried out under 25 °C using a Xe lamp solar simulator (Newport, 94063A-1000, 100 mW/cm²) coupled with an air mass 1.5 global (AM 1.5G) filter, and the EQE measurements were characterized by a commercial spectral response system (PV Measurement Inc. QEX10). The reliability of solar cells under multiple bending cycles were performed with a home-built automatic bending setup.

Supporting Information

Supporting Information is available from the Wiley Online Library or from the author.

Acknowledgements

This work was financially supported by the National Natural Science Foundation of China (61622407, 61474128, 21503261, 61504155), Science & Technology Commission of Shanghai Municipality (14JC1492900, 16DZ1207300), the Youth Innovation Promotion Association, Chinese Academy of Sciences (2013302) and the Youth Innovation Fund for Interdisciplinary Research of Shanghai Advanced Research Institute (Y526453233), and the Priority Academic Program Development (PAPD) of Jiangsu Higher Education Institutions.

Received: September 11, 2016

Revised: December 9, 2016

Published online: February 10, 2017

- [1] A. V. Shah, R. Platz, H. Keppner, *Sol. Energy Mater. Solar Cells* **1995**, 38, 501.
- [2] F. J. Haug, C. Ballif, *Energy Environ. Sci.* **2015**, 8, 824.
- [3] Q. Lin, H. Huang, Y. Jing, H. Fu, P. C. Chang, D. Li, Y. Yao, Z. Fan, *J. Mater. Chem. C* **2014**, 2, 1233.
- [4] M. B. Schubert, J. H. Werner, *Mater. Today* **2006**, 9, 42.
- [5] J. H. Petermann, D. Zielke, J. Schmidt, F. Haase, E. G. Rojas, R. Brendel, *Prog. Photovoltaics* **2012**, 20, 1.
- [6] W. Schmidt, B. Woesten, J. P. Kalejs, *Prog. Photovoltaics* **2002**, 10, 129.
- [7] C. Y. Lee, C. M. Yeh, Y. T. Liu, C. M. Fan, C. F. Huang, Y. R. Wu, *J. Renewable Sustainable Energy* **2014**, 6, 1829.
- [8] S. F. Leung, Q. Zhang, F. Xiu, D. Yu, J. C. Ho, D. Li, Z. Fan, *J. Phys. Chem. Lett.* **2014**, 5, 1479.
- [9] R. Biron, S. Hanni, M. Boccard, C. Pahun, K. Soderstrom, M. Duchamp, R. Dunin-Borkowski, G. Bugnon, L. Ding, S. Nicolay, G. Parascandolo, F. Meillaud, M. Despeisse, F. J. Haug, C. Ballif, *Sol. Energy Mater. Solar Cells* **2013**, 114, 147.
- [10] H. Sai, M. Kondo, *Conf. Rec. IEEE Photovoltaic Spec. Conf.* **2010**, 295, 000295.
- [11] C. Yang, C. Y. Hsueh, D. J. Yeh, C. I. Ho, C. M. Leu, Y. H. Yeh, S. C. Lee, *IEEE Electron Device Lett.* **2011**, 32, 1254.
- [12] Z. Fan, R. Kapadia, P. W. Leu, X. Zhang, Y. L. Chueh, K. Takei, K. Yu, A. Jamshidi, A. A. Rathore, D. J. Ruebusch, M. Wu, A. Javey, *Nano Lett.* **2010**, 10, 3823.
- [13] D. Yu, M. Yin, L. Lu, H. Zhang, X. Chen, X. Zhu, J. Che, D. Li, *Adv. Mater.* **2015**, 27, 6747.
- [14] Z. Fan, H. Razavi, J. W. Do, A. Moriwaki, O. Ergen, Y. L. Chueh, P. W. Leu, J. C. Ho, T. Takahashi, L. A. Reichertz, S. Neale, K. Yu, M. Wu, J. W. Ager, A. Javey, *Nat. Mater.* **2009**, 8, 648.
- [15] S. Jeong, E. C. Garnett, S. Wang, Z. Yu, S. Fan, M. L. Brongersma, M. D. McGehee, Y. Cui, *Nano Lett.* **2012**, 12, 2971.
- [16] K. H. Tsui, Q. Lin, H. Chou, Q. Zhang, H. Fu, P. Qi, Z. Fan, *Adv. Mater.* **2014**, 26, 2805.
- [17] S. F. Leung, L. Gu, Q. Zhang, K. Tsui, J. M. Shieh, C. Shen, T. H. Hsiao, C. H. Hsu, L. Lu, D. Li, Q. Lin, Z. Fan, *Sci. Rep.* **2014**, 4, 1154.
- [18] Y. Liao, Y. Wang, Y. Yen, C. Chen, D. H. Hsieh, S. Chen, C. Y. Lee, C. Lai, W. Kuo, J. Y. Juang, K. Wu, S. J. Cheng, C. Lai, F. Lai, S. Kuo, H. Kuo, Y. L. Chueh, *ACS Nano* **2013**, 7, 7318.
- [19] H. Lin, F. Xiu, M. Fang, S. Yip, H. Y. Cheung, F. Wang, N. Han, K. S. Chan, C. Y. Wong, J. C. Ho, *ACS Nano* **2014**, 8, 3752.
- [20] H. Xiao, J. Wang, H. Huang, L. Lu, Q. Lin, Z. Fan, X. Chen, C. Jeong, X. Zhu, D. Li, *Nano Energy* **2015**, 11, 78.
- [21] H. Huang, L. Lu, J. Wang, J. Yang, S. F. Leung, Y. Wang, D. Chen, X. Chen, G. Shen, D. Li, Z. Fan, *Energy Environ. Sci.* **2013**, 6, 2965.
- [22] B. Liu, X. Liang, J. Liang, L. Bai, H. Gao, Z. Chen, Y. Zhao, X. Zhang, *Nanoscale* **2015**, 7, 9816.
- [23] H. Sai, H. Fujiwara, M. Kondo, Y. Kanamori, *Appl. Phys. Lett.* **2008**, 93, 143501.
- [24] H. Sai, M. Kondo, *J. Appl. Phys.* **2009**, 105, 094511.
- [25] H. Sai, M. Kondo, *Sol. Energy Mater. Solar Cells* **2011**, 95, 131.
- [26] H. Sai, K. Saito, M. Kondo, *Appl. Phys. Lett.* **2012**, 101, 173901.
- [27] H. Sai, T. Koida, T. Matsui, I. Yoshida, K. Saito, M. Kondo, *Appl. Phys. Express* **2013**, 6, 104101.
- [28] C. Genet, T. W. Ebbesen, *Nature* **2007**, 445, 39.
- [29] S. F. Leung, M. Yu, Q. Lin, K. Kwon, K. L. Ching, L. Gu, K. Yu, Z. Fan, *Nano Lett.* **2012**, 12, 3682.
- [30] A. Mavrokefalos, S. E. Han, S. Yerci, M. S. Branham, G. Chen, *Nano Lett.* **2012**, 12, 2792.
- [31] V. E. Ferry, L. A. Sweatlock, D. Pacifici, H. A. Atwater, *Nano Lett.* **2008**, 8, 4391.
- [32] R. A. Pala, J. White, E. Barnard, J. Liu, M. L. Brongersma, *Adv. Mater.* **2009**, 21, 3504.
- [33] R. B. Dunbar, H. C. Hesse, D. S. Lembke, L. Schmidt-Mende, *Phys. Rev. B* **2012**, 85, 035301.
- [34] N. N. Lal, H. Zhou, M. Hawkeye, J. K. Sinha, P. N. Bartlett, G. A. J. Amarantunga, J. J. Baumberg, *Phys. Rev. B* **2012**, 85, 245318.
- [35] Y. Lin, Z. Xu, D. Yu, L. Lu, M. Yin, M. M. Tavakoli, X. Chen, Y. Hao, Z. Fan, Y. Cui, *ACS Appl. Mater. Interfaces* **2016**, 8, 10929.
- [36] C. M. Hsu, C. Battaglia, C. Pahun, Z. C. Ruan, F. J. Haug, S. H. Fan, C. Ballif, Y. Cui, *Adv. Energy Mater.* **2012**, 2, 628.
- [37] H. Sai, H. Fujiwara, M. Kondo, Y. Kanamori, *Appl. Phys. Lett.* **2008**, 93, 143501.
- [38] Q. Lin, S. F. Leung, L. Lu, X. Chen, Z. Chen, H. N. Tang, W. J. Su, D. Li, Z. Fan, *ACS Nano* **2014**, 8, 6484.
- [39] S. F. Leung, K. H. Tsui, Q. Lin, H. Huang, L. Lu, J. M. Shieh, C. Shen, C. H. Hsu, Q. Zhang, D. Li, Z. Fan, *Energy Environ. Sci.* **2014**, 7, 3611.
- [40] Q. Lin, L. Lu, M. M. Tavakoli, C. Zhang, G. C. Lui, Z. Chen, X. Chen, L. Tang, D. Zhang, Y. Lin, P. Chang, D. Li, Z. Fan, *Nano Energy* **2016**, 22, 539.

- [41] M. Sun, Z. Xu, M. Yin, Q. Lin, L. Lu, X. Xue, X. Zhu, Y. Cui, Z. Fan, Y. Ding, L. Tian, H. Wang, X. Chen, D. Li, *Nanoscale* **2016**, *8*, 8924.
- [42] J. van de Groep, P. Spinelli, A. Polman, *Nano Lett.* **2015**, *15*, 4223.
- [43] C. Peroz, V. Chauveau, E. Barthel, E. Sondergard, *Adv. Mater.* **2009**, *21*, 555.
- [44] K.-Y. Yang, K.-M. Yoon, K.-W. Choi, H. Lee, *Microelectron. Eng.* **2009**, *86*, 2228.
- [45] M. A. Verschuuren, *Acta Crystallogr.* **2010**, *62*, 1671.
- [46] B. Hua, Q. F. Lin, Q. P. Zhang, Z. Y. Fan, *Nanoscale* **2013**, *5*, 6627.
- [47] J. Yang, H. Huang, Q. Lin, L. Lu, X. Chen, L. Yang, X. Zhu, Z. Fan, Y. Song, D. Li, *ACS Appl. Mater. Interfaces* **2014**, *6*, 2285.
- [48] C. Yang, Y. Qin, X. Zhu, M. Yin, D. Li, X. Chen, Y. Song, *J. Alloys Compd.* **2015**, *632*, 634.
- [49] C. E. Bouldin, W. E. Wallace, G. W. Lynn, S. C. Roth, W. L. Wu, *J. Appl. Phys.* **2000**, *88*, 691.
- [50] Ube Industries, Ltd, Chemicals: Polyimide,UPILEX®-S, 2016(6),
- [51] M. O. Reese, S. A. Gevorgyan, M. Jorgensen, E. Bundgaard, S. R. Kurtz, D. S. Ginley, D. C. Olson, M. T. Lloyd, P. Moryillo, E. A. Katz, A. Elschner, O. Haillant, T. R. Currier, V. Shrotriya, M. Hermenau, M. Riede, K. R. Kirov, G. Trimmel, T. Rath, O. Inganäs, F. L. Zhang, M. Andersson, K. Tvingstedt, M. Lira-Cantu, D. Laird, C. McGuinness, S. Gowrisanker, M. Pannone, M. Xiao, J. Hauch, R. Steim, D. M. DeLongchamp, R. Rosch, H. Hoppe, N. Espinosa, A. Urbina, G. Yaman-Uzunoglu, J. B. Bonekamp, A. J. J. M. van Breemen, C. Girotto, E. Voroshazi, F. C. Krebs, *Sol. Energy Mater. Solar Cells* **2011**, *95*, 1253.
- [52] R. Guo, H. Huang, P. C. Chang, L. Lu, X. Chen, X. Yang, Z. Fan, B. Zhu, D. Li, *Nano Energy* **2014**, *8*, 141.
- [53] C. van Lare, F. Lenzmann, M. A. Verschuuren, A. Polman, *Nano Lett.* **2015**, *15*, 4846.
- [54] F. J. Haug, T. Soderstrom, M. Python, V. Terrazzoni-Daudrix, X. Niquille, C. Ballif, *Sol. Energy Mater. Solar Cells* **2009**, *93*, 884.
- [55] T. Soderstrom, F. J. Haug, V. Terrazzoni-Daudrix, C. Ballif, *J. Appl. Phys.* **2010**, *107*, 014507.
- [56] Y. Ichikawa, T. Yoshida, T. Hama, H. Sakai, K. Harashima, *Sol. Energy Mater. Solar Cells* **2001**, *66*, 107.
- [57] K. Nomura, H. Ohta, A. Takagi, T. Kamiya, M. Hirano, H. Hosono, *Nature* **2004**, *432*, 488.
- [58] Y. Leterrier, L. Medico, F. Demarco, J. A. E. Manson, U. Betz, M. F. Escola, M. K. Olsson, F. Atamny, *Thin Solid Films* **2004**, *460*, 156.
- [59] H. B. Jo, J. Choi, K. J. Byeon, H. J. Choi, H. Lee, *Microelectron. Eng.* **2014**, *116*, 51.
- [60] E. D. Palik, *J. Opt. Soc. Am.* **1984**, *1*, 1297.